ENVIRONMENT MAPPING AND ROBUST LOCALIZATION FOR MOBILE ROBOTS NAVIGATION IN INDOOR ENVIRONMENTS

Geovany Araújo Borges*, Marie-José Aldon†

*Grupo de Instrumentação, Controle e Automação (GICA)
Departamento de Engenharia Elétrica (ENE) - Universidade de Brasília (UnB)
Caixa Postal 04591 - Asa Norte - Brasilia - CEP 70910-900 - Brazil

†Département Robotique - LIRMM
UMR CNRS/Université Montpellier II, nº. C55060
161, rue ADA. 34392 - Montpellier - Cedex 5 - France

Emails: gaborges@ene.unb.br, aldon@lirmm.fr

Abstract— This work presents an overall description of a Concurrent Mapping and Localization system implanted on a mobile robot. Its main contributions were on original robust methods for map-based localization and stochastic mapping. In order to increase robustness on map-based localization, a new technique based on robust M-estimators was proposed. With a new approach for environment mapping using stochastic constraints between map structures, reduced map divergence was verified in experiments. Comparisons of the proposed robust methods against classic Kalman filtering-based approaches were carried out in real environments.

Keywords— Concurrent Mapping and Localization, Mobile robotics, robust estimation, multisensory system.

Resumo— Nesse trabalho é apresentada uma descrição geral de um sistema de Localização e Cartografia Concorrentes que foi implantado em um robô móvel. Suas principais contribuições foram em métodos originais de localização e cartografia estocástica. Como forma de aumentar a robustez da localização baseada em mapas de ambiente, uma nova técnica usando M-estimadores robustos foi derivada. Com uma nova abordagem para cartografia de ambientes usando restrições estocásticas verificou-se, experimentalmente, reduzida divergência dos mapas construídos. São ainda apresentadas comparações entre os métodos propostos e técnicas clássicas baseadas em filtragem de Kalman.

Keywords— Localização e Cartografia Concorrentes, Robótica móvel, estimação robusta, sistema multisensorial.

1 Introduction

Concurrent Mapping and Localization (CML) is a very active subject of research on mobile robotics, with numerous solutions proposed in the two last decades. In this context, the initial most important contributions were (Moravec and Elfes, 1985; Smith et al., 1990; Leonard et al., 1992). In CML, a mobile robot explores an previously unknown environment and builds an internal representation of it, in the form of an environment map. Depending on the environment map representation, there exist solutions for topological (Kuipers and Byan, 1991), grid (Thrun et al., 1998), and geometrical-based maps (Leonard and Feder, 2000). The environment map is used simultaneously for robot localization, making the two processes concurrent. Such a coupling between mapping and localization makes the system very sensitive to deterministic and stochastic errors in the involved estimation procedures.

This work presents an overall description of a CML system implanted on a real mobile robot, described in more details in (Borges, 2002). Its main contributions were on original robust methods for map-based localization (Borges and Aldon, 2003) and stochastic mapping (Borges and Aldon, 2002). The paper is organized as follows. Section 2 introduces the mobile robot used in this work, on which the proposed CML system, presented in section 3, was implanted. Experimental evaluations are in section 4, followed by concluding remarks in section 5.

2 Mobile platform

The mapping and localization system presented in this work was implanted on the Omni, developed at LIRMM, in France (*c.f.* Fig. 1). Each wheel has two motion axis, one for orientation and one for traction. Its hardware architecture is controlled by a Pentium™ II 300 MHz IBM-PC microcomputer, which interfaces to its sensorial apparatus and actuators through I/O cards and high-speed serial links. As proprioceptive sensors, there are (i) six incremental optical encoders, one for each motion axis, (ii) three absolute encoders, one for each wheel orientation axis, and (iii) a high precision laser gyrometer (drift less than $45^{\circ}/h$). The exteroceptive sensors are (i) a monochrome video camera and (ii) a rotating laser rangefinder, manufactured by IBEO Lasertechnik, with a maximum range of 30 m a ± 0.05 m accuracy. This sensor provides scans in a 270° angular field with a resolution of 0.6° at 8 images per second.

Omni's kinematic model is derived based on the rolling without slipping constraint at the wheel/ground contact point (Campion et al.,

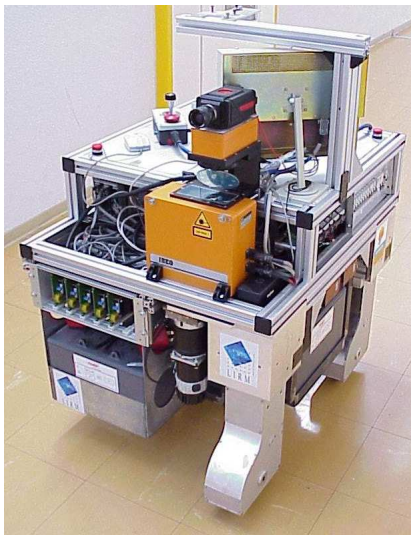

Figure 1: The Omni mobile platform.

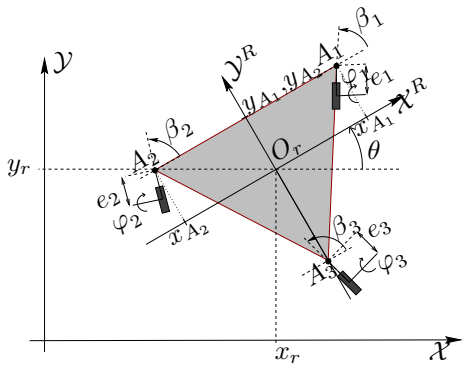

Figure 2: Omni geometric parameters.

1996). The describing parameters of its configuration kinematic model is shown in Figure 2. Considering the *i-th* wheel, the geometric parameters are its radii r_i, its offset e_i, and the coordinates (x_{A_i}, y_{A_i}) of the wheel direction axis A_i in the two-dimensional robot frame. Its configuration is described by the direction angle β_i and the posture angle φ_i. Considering the three axis mechanism, the model geometrical parameters are all stacked in vector $\boldsymbol{\lambda}$. Let $\mathbf{q} = (\beta_1, \beta_2, \beta_3, \varphi_1, \varphi_2, \varphi_3)^T$ be the robot configuration parameters. The Omni kinematic model given by

$$\dot{\mathbf{q}} = \mathbf{J}(\mathbf{q}, \boldsymbol{\lambda}, \boldsymbol{\theta}) \cdot \dot{\mathbf{z}}. \qquad (1)$$

with $\mathbf{z} = (x, y, \theta)^T$ being the robot coordinates in the world frame and $\mathbf{J}$ being the Jacobian matrix, whose pseudo-inverse exist for any robot configuration. This brings the robot its omnidirectional capability.

3 System description

The main modules of the localization and mapping architecture are illustrated in Figure 3. In such a system, a robot pose estimated is updated at high rates (5 ms sampling time) using dead-reckoning. Due to accumulated dead-reckoning errors, the robot pose is corrected during periodic map-based pose estimation cycles, in this case every two seconds. A cycle encompasses: exteroceptive sensor data acquisition, image processing, local mapping and pose estimation. Once global pose estimation is concluded, a (global) map updating is performed. This architecture is almost the same of most mobile robotic systems. Indeed, its originality resides in each module, discussed in the sequel.

3.1 Dead-reckoning

Dead-reckoning encompasses pose estimation techniques which integrate data gathered from proprioceptive sensors. Since no world reference can be given by such sensors, pose estimate uncertainty increases with time. The most known dead-reckoning technique used in mobile robots is odometry. It integrates the robot kinematic model using motion information derived from axis incremental encoders. Due to modeling errors and approximate geometric parameters, odometry diverges rapidly. In order to minimize this, parameter identification using extended Kalman filtering was applied off-line to obtain a better estimate for $\boldsymbol{\lambda}$. In this procedure, the Omni's laser gyrometer provided high precision $\dot{\theta}$ measurements used for updating the parameters estimate. It resulted in an important accuracy enhancement of odometry.

It has been observed that small errors on θ, propagated through odometry's equations, have a great impact on accuracy. In order to achieve more accurate dead-reckoning, an other dead-reckoning technique has been implanted: gyrodometry. In this technique, θ estimate is obtained by directly integrating the accurate $\dot{\theta}$ measurements provided by a laser gyrometer. Robot position (x, y) is estimated using a reduced form of Eq. (1).

3.2 Sensor data acquisition

This module performs the first procedures of a localization cycle. It performs real-time, synchronized data acquisition of a pair of laser rangefinder and video camera images, named $\mathcal{L}$ and $\mathcal{I}$, respectively. As pre-processing procedures, (i) $\mathcal{L}$ is compensated from robot motion during sensor scanning, (ii) $\mathcal{L}$ is applied to local geometrical transformations in order to bring it to the instant when $\mathcal{I}$ was acquired, using recorded dead-reckoning data. These procedures are necessary in order to have exteroceptive data coherent with the robot local environment.

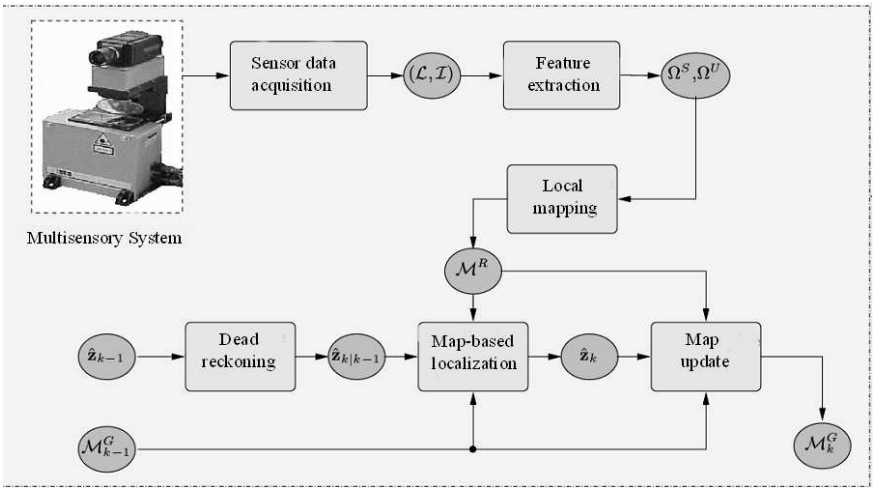

Figure 3: Procedures of the map building and localization system

3.3 Feature extraction

Feature extraction creates two lists Ω^S and Ω^U of geometric primitives extracted from $\mathcal{L}$ and $\mathcal{I}$. From $\mathcal{L}$, a set Ω^S of line segments is extracted by using the robust split-and-merge fuzzy algorithm (Borges and Aldon, 2000). Further, laser scan breakpoints are detected using an extended Kalman filter-based approach (Castellanos and Tardós, 1996). Breakpoints correspond to important discontinuities in the laser scan sequence, and may indicate the extremities of local environment surfaces. From image $\mathcal{I}$, similarly to (Arras et al., 2001), a set Ω^U of vertical line segments is extracted, which correspond to strong vertical contours in the image.

3.4 Local mapping

Given the set Ω^S obtained from the range image, an initial local map $\mathcal{M}^R$ is built. Such a map is composed of semiplanes (lines segments with side of view), edges (semiplane extremities) and corners (the crossing point of two semiplanes). Semiplanes are obtained from all line segments of Ω^S. Edges are computed from scan points which are (i) support points of line segments, and (ii) breakpoints. Edges are the projections on the support line segment of all scan points which satisfy (i) and (ii). Corners are the intersection of all line segments supported by consecutive scan points which are not breakpoints.

A calibration procedure allowed to relate the horizontal coordinate u of a video vertical line to its angle of view ϕ in the laser rangefinder reference frame (Borges, 2002). This relationship is given by an affine model, used to find correspondences between the video vertical features and edges. This is model is also explored int the second phase of local map, which uses the vertical lines extracted from the video image to update the initial local map structures. For last, photometric edges are estimated from all vertical lines which did not have correspondences in the initial local map. Since these structures are composed of a point, and the camera can only capture their observation angle ϕ, they are estimated using bootstrap samples, obtained from the distribution of all scan points which lie, according to the Mahalanobis distance test, in the same angle of view of the vertical line. Photometric edges presenting large covariance matrices are discarded. Figure 4 shows a local map $\mathcal{M}^R$ obtained from laser and video images.

3.5 Map-based localization

This module performs absolute robot pose estimation (corrects dead-reckoning) from corresponding structures of maps $\mathcal{M}^R$ and $\mathcal{M}^G_{k-1}$ (current global map, updated in the last localization cycle at discrete time $k-1$). Classical methods based on Kalman filtering lack of robustness and difficulties associated to convergence is a critical problem. New approaches based on guaranteed optimal estimation and linear Kalman filtering were proposed in our previous research on the subject (Borges and Aldon, 2003). In these approaches, local map matching between $\mathcal{M}^R$ and $\mathcal{M}^G_{k-1}$ results in a set of corresponding low-level geometrical features (lines and points). From such features, an optimal estimate of the robot pose in the weighted least squares sense are obtained. Such estimate $\hat{\mathbf{z}}$ minimize

$$J(\mathbf{z},\mathcal{U}) = \sum_{n=1}^{N} \mu_n \cdot \|\mathbf{r}_n\|^2 , \qquad (2)$$

where $\mathcal{U}$ represents the set of N feature correspondences. $\mathbf{r}_n$ is the residual of the *n-th* correspondence defined in a common representation for both types of features. μ_n is a positive weighting factor, computed using robust weighting functions (Huber, 1981). Such functions allow the al-

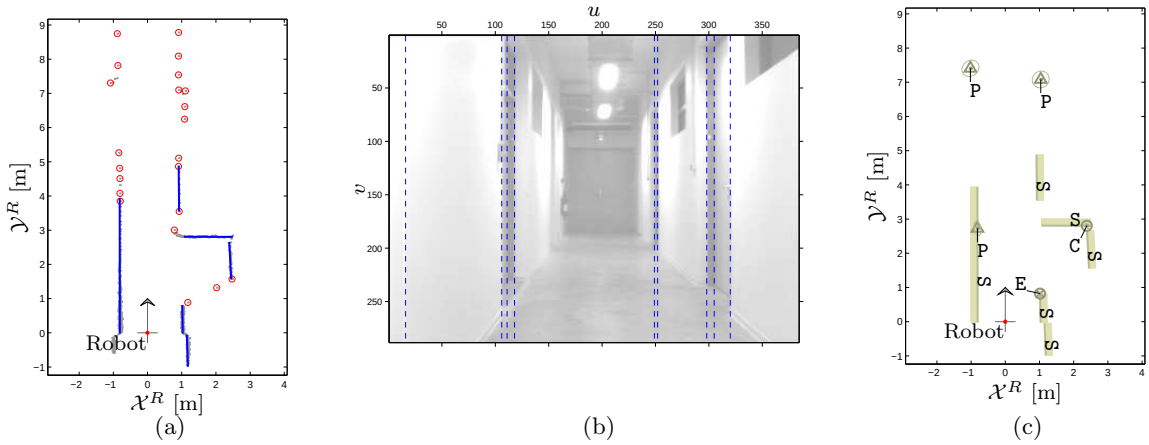

(a) (b) (c)

Figure 4: Local map building example. (a) Range image and features (line segments and breakpoints). (b) Video image and features (vertical lines). (c) Local map (S: Semiplanes, E: Edges, C: Corners, and P: Photometric edges)

gorithm to reject (i.e., $\mu \to 0$) feature correspondences which are unlikely to be in agreement with the entire set of correspondences, as in cluttered environments. The minimization of the cost function Eq. (2) is performed iteratively, resulting in M-Estimators. The covariance matrix associated with the pose estimate is also computed. Since this procedure takes some time, the estimated pose is updated to the current time by integrating robot motion during this module execution time.

3.6 Map update

In this procedure, structures of $\mathcal{M}^G_{k-1}$ are updated using the local observations at $\mathcal{M}^R$ and the estimated pose, resulting in $\mathcal{M}^G_k$. This is achieved using a decoupled map updating estimator (Borges and Aldon, 2002), which propagates stochastic constraints in order to minimize map divergence. Such constraints do exist in local map structures (*e.g.*, and edge is over a semiplane), and should be preserved in the global map $\mathcal{M}^G_k$. This has been achieved from a rigorous theoretical analysis of Kalman filter and the use of covariance intersection filter (Julier and Uhlmann, 1997). It should be pointed out that map-based localization and map update modules are independent. It means that, on the contrary of well known simultaneous map building and localization approaches (Dissanayake et al., 2001)(Leonard et al., 1992), which are coupled ones, the proposed modules do not keep correlations between the robot pose and the map structures. This reduces the overall system complexity and computing time. This is in counter sense of the well established idea that correlations exist between pose and map structures, and they should be estimated in order to achieve consistent mapping. The idea we defend is that by applying new stochastic estimation techniques, reliable and consistent mapping and localization can be achieved.

4 Experimental evaluations

This section presents few results from experimental evaluations of (i) map-based pose estimation and (ii) concurrent localization and mapping. For more evaluations, please refer to (Borges, 2002).

4.1 Pose estimation

In order to evaluate the proposed map-based pose estimators, an experiment in a long narrow corridor has been carried out. In this experiment, Omni has followed a trajectory on which high translational and rotational speeds have been verified. Some data of the experiment are shown in Figure 5, including four video images. The environment map was provided by our mapping technique, but with accurate gyrodometry used as pose estimator. This makes the pose estimator and the environment map uncorrelated, leading to an unbiased evaluation. Further, the entire experimental data have been firstly acquired, and the pose estimators were evaluated offline, under the same conditions.

The offsets $\hat{\varepsilon}_x$, $\hat{\varepsilon}_y$ and $\hat{\varepsilon}_\theta$ of pose parameters (x, y, θ) with respect to gyrodometry are presented on Figure 6. Thus, gyrodometry is also used as reference pose for comparison. This figure contains the results of two different estimators: the sequential extended Kalman filter, commonly used for geometrical map-based robot localization, and our robust M-estimator, named μ-Huber. The $\pm 3\sigma$ limits, computed from the estimated error covariance matrix, are represented in gray. The classical Kalman filtering approach has presented statistical divergence on x estimation starting from the *50th* localization cycle. This divergence has been propagated to the other variables, leading the robot to get completely lost after few cycles. Such divergence is probably due to the presence of false matchings (outliers) between the local and

(a) Experiment data

Number of localization cycles :	75		
Experiment total time :	150,6 s	Translational maximum velocity:	91,83 cm/s
Total displacement :	85,38 m	Rotational maximum velocity:	39,4 $^\circ/s$

(b) Images corresponding to some strategic points in the robot trajectory

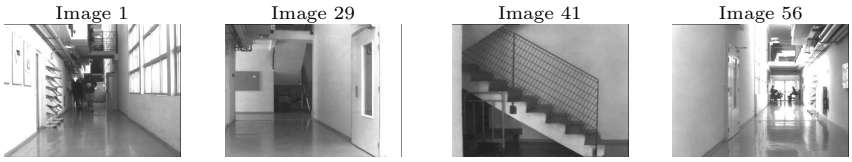

(c) Global environmente map and robot trajectory

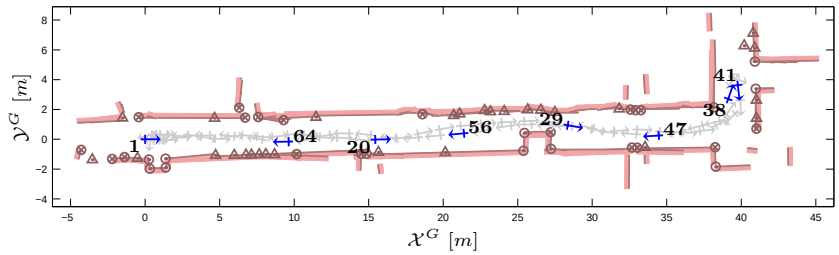

Figure 5: Experimental evaluation contitions of pose estimation

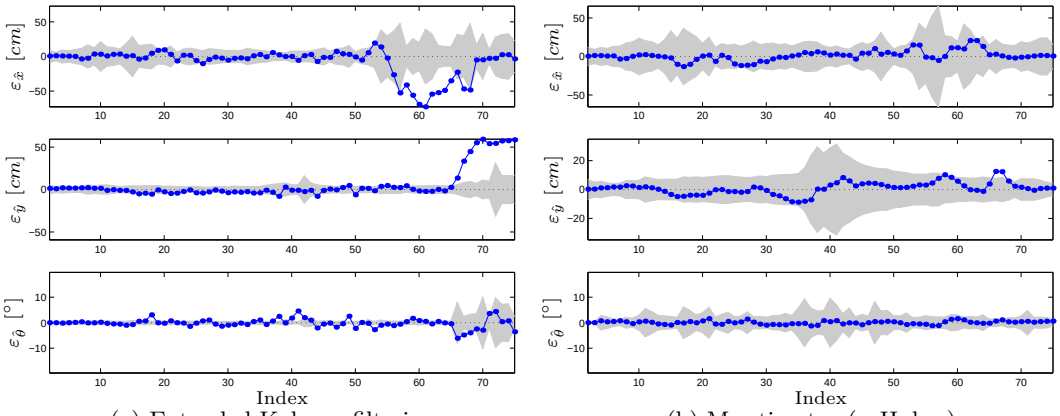

(a) Extended Kalman filtering (b) M-estimator (μ-Huber)

Figure 6: Offsets of the pose estimates with respect to gyrodometry, and $\pm 3\sigma$ confidence intervals.

the global map. The robust M-estimator in Figure 6(b) did not diverged. At about the same localization cycle on which the preceding approach diverged, the robust estimator presented statistical estimation consistency, *i,e.*, offsets inside the $\pm 3\sigma$ limits. In the whole experiment, estimated uncertainty of the robust approach is larger than that of Kalman filter, reflecting the difficulty level of the experiment. Indeed, in narrow corridors and at high speeds, errors occur more frequently.

4.2 Concurrent localization and environment mapping

In this section, the proposed decoupled stochastic propagation approach is compared against the classical decoupled extended Kalman filtering one. It is well known that the convergence of mapping approaches can be evaluated in experiments on closed loop environments. Thus, in the proposed comparison, Omni navigated in an environment with such characteristic, gathering data for offline evaluation. The results are presented in Figure 7. Dead-reckoning is provided by odometry only, which is likely to introduce larger localization errors. Fig. 7(a) shows the map obtained using the classical Kalman filtering approach. It is notorious that this approach presented a large divergence in this experiment. The proposed approach presented satisfactory results in Figure 7(b). This method used robust M-estimator (see previous section) for pose estimation. Since concurrent localization and mapping is very sensitive to errors at any component of the system, the better results of Figure 7(b) are also in consequence of a superior performance of the localization and mapping architecture.

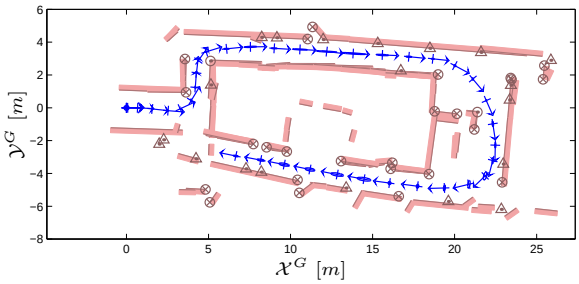

(a) Classical decoupled approach using extended Kalman filtering

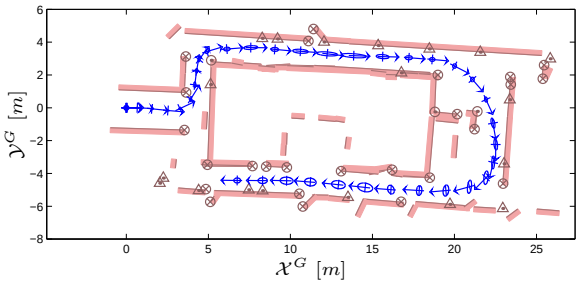

(b) Proposed decoupled approach based on stochastic constraints

Figure 7: Experimental results of concurrent localization and mapping.

5 Conclusions

This paper presented the main contributions of (Borges, 2002) in the field of Concurrent Mapping and Localization. The presented solutions were extensively evaluated on a real mobile platform, the Omni robot. Currently, this robot has been borrowed to *Universidade de Brasilia*, covered by an agreement with *Université Montpellier II*. The current research is focused on trajectory planning, obstacle avoidance and visual navigation.

Acknowledgements

During this work G. A. Borges was supported by CAPES under grant BEX2280/97-3

References

Arras, K. O., Tomatis, N., Jensen, B. T. and Siegwart, R. (2001). Multisensor on-the-fly localization: Precision and reliability for applications, *Robotics and Autonomous Systems* **34**: 131–143.

Borges, G. A. (2002). *Cartographie de l'environnement et localisation robuste pour la navigation de robots mobiles*, PhD thesis, Université Montpellier II, LIRMM, 161 rue ADA, 34392, Montpellier, Cedex 5, France. *One of the recipients of the 2001/2002 Club EEA prize for the best french thesis in Automatic Control.*

Borges, G. A. and Aldon, M.-J. (2000). A split-and-merge segmentation algorithm for line extractions in 2-D range images, 15^{th} *International Conference on Pattern Recognition.*

Borges, G. A. and Aldon, M.-J. (2002). A decoupled approach for simultaneous stochastic mapping and mobile robot localization, *IEEE/RSJ International Conference on Intelligent Robots and Systems.*

Borges, G. A. and Aldon, M.-J. (2003). Robustified estimation algorithms for mobile robot localization based on geometrical environment maps, *Robotics and Autonomous Systems* **45**(3-4): 131–159.

Campion, G., Bastin, G. and D'Andréa-Novel, B. (1996). Structural properties and classification of kinematic and dynamic models of wheeled mobile robots, *IEEE Transactions on Robotics and Automation* **12**(1): 47–62.

Castellanos, J. A. and Tardós, J. D. (1996). Laser-based segmentation and localization for a mobile robot, *in* F. P. M. Jamshidi and P. Dauchez (eds), *Robotics and Manufacturing: Recent Trends in Research and Applications*, Vol. 6, ASME Press, pp. 101–109.

Dissanayake, M. W. M. G., Newman, P., Clark, S., Durrant-Whyte, H. F. and Csorba, M. (2001). A solution to the simultaneous localization and map building (SLAM) problem, *IEEE Transactions on Robotics and Automation* **17**(3): 229–241.

Huber, P. J. (1981). *Robust Statistics*, John Wiley & Sons.

Julier, S. J. and Uhlmann, J. K. (1997). A non-divergent estimation algorithm in the presence of unknown correlations, *American Control Conference.*

Kuipers, B. and Byan, Y. T. (1991). A robot exploration and mapping strategy based on a semantic hierarchy of spatial representations, *Journal of Robotics and Autonomous Systems* **8**: 47–63.

Leonard, J. J., Durrant-Whyte, H. F. and Cox, I. J. (1992). Dynamic map building for an autonomous mobile robot, *The International Journal of Robotics Research* **11**(4): 286–298.

Leonard, J. J. and Feder, H. J. S. (2000). A computationally efficient method for large-scale concurrent mapping and localization, *Proceedings of the Ninth International Symposium on Robotics Research*, pp. 169–176.

Moravec, H. P. and Elfes, A. (1985). High resolution maps from wide angle sonar, *IEEE International Conference on Robotics and Automation*, pp. 116–121.

Smith, R., Self, M. and Cheeseman., P. (1990). Estimating uncertain spatial relationships in robotics, *in* I. J. Cox and G. T. Wilfong (eds), *Autonomous Robot Vehicles*, Springer Verlag, pp. 167–193.

Thrun, S., Fox, D. and Burgard, W. (1998). A probabilistic approach to concurrent mapping and localization for mobile robots, *Machine Learning* **31**: 29–53.